European Polymer Journal 72 (2015) 202–211

Contents lists available at ScienceDirect

European Polymer Journal

journal homepage: www.elsevier.com/locate/europolj

Macromolecular Nanotechnology

Magnetic characterization of chitosan–magnetite nanocomposite films

Gianina A. Kloster [a], Diego Muraca [b], Cintia Meiorin [a,b], Kleber R. Pirota [b], Norma E. Marcovich [a], Mirna A. Mosiewicki [a,*]

[a] Institute of Material Science and Technology (INTEMA), National University of Mar del Plata-National Research Council (CONICET), Juan B. Justo 4302, 7600 Mar del Plata, Argentina
[b] Institute of Physics Gleb Wataghin, University Estadual de Campinas, CEP 13083-859 Campinas, SP, Brazil

ARTICLE INFO

Article history:
Received 3 July 2015
Received in revised form 10 September 2015
Accepted 16 September 2015
Available online 24 September 2015

Keywords:
Nanomagnetite
Magnetic properties
Chitosan films
Plasticizer

ABSTRACT

Magnetic nanocomposites using chitosan as a matrix and magnetite nanoparticles (MNP) generated "in situ" were prepared and magnetically characterized. The content of nanoparticles on the composites was varied from 2 to 10 wt.% and their effects, as well as the addition of 30 wt.% of glycerol as plasticizer in the formulation, were analyzed. The magnetization properties were evaluated using the zero field cooling/field cooling (ZFC/FC) measurements and magnetization loops obtained at different temperatures. The results showed that magnetization at high field (20 KOe) and coercivity increase with magnetite content. Super-paramagnetic behavior was observed for all non-plasticized samples with exception of the film with 2 wt.% of magnetite. Glycerol affected significantly the composite magnetization values and the magnetic interactions between particles, which are reflected in the blocking and irreversibility temperatures of the different systems. Moreover, the size of the precipitated magnetic nanoparticles depends on their concentration as well as on the addition of plasticizer to the formulation, as was corroborated by TEM and SAXS measurements.

1. Introduction

Magnetic nanocomposites from polymeric matrix have attracted scientific interest due to the potential applications in diverse areas such as biomedicine, biotechnology and materials science among others. If the polymer matrix is a biopolymer, several advantages are incorporated to the obtained material, like biodegradability, biocompatibility and use of renewable resources with the consequent decrease in the environmental impact.

Among a variety of biopolymers, chitosan presents excellent film forming capability, high mechanical strength, biocompatibility, non-toxicity, bactericide effect, high permeability toward water, susceptibility to chemical modifications, cost-effectiveness, etc. [1,2]. Chitosan is a natural cationic polysaccharide obtained from N-deacetylation of chitin, a major component of crustacean shells and fungal biomass and it is readily available from seafood processing wastes [2,3]. It is widely used in tissue engineering and magneto hyperthermia applications [4] but also, because of its high amino content, it has been found to possess good sorption capacity for many heavy metal ions through complexation with the amine groups and has been widely used as biosorbent for removing various metal ions from wastewater [3].

* Corresponding author.
E-mail address: mirna@fi.mdp.edu.ar (M.A. Mosiewicki).

http://dx.doi.org/10.1016/j.eurpolymj.2015.09.014
0014-3057/

On the other hand, colloidal inorganic nanometer-sized particles or nanocrystals have proved to be useful as building blocks for the development of nanomaterials and biomaterials in nanoscience and biotechnology. Their unique physical and optical properties are attributed to nanoscale phenomena [5]. Superparamagnetic iron oxide including magnetite (Fe_3O_4) and maghemite (γFe_2O_3) have great potential for various biomedical and biotechnological applications because of their chemical stability, biodegradability and low toxicity [6,7]. They include magnetic resonance imaging, contrast enhancement, targeted drug delivery, hyperthermia, catalysis, biological separation, biosensors, and diagnostic medical devices [8–10].

Although magnetic nanoparticles have been synthesized and studied from several years, its incorporation to biopolymers to generate functional nanocomposites is a relatively new area of study. The dispersion of the particles in the polymeric matrix can strongly influence the magnetic properties of the films and thus, the study of the actual magnetic response of final materials is of vital importance to define potential applications. Thereby, considering the previous work about the synthesis and characterization (physical, thermal and mechanical) of chitosan/magnetite nanocomposites [11], the aim of this work is to analyze specifically, the magnetic properties of nanocomposite films made from chitosan (with and without glycerol added as plasticizer) with different content of magnetic nanoparticles.

2. Experimental

2.1. Materials

Chitosan (CS) (degree of deacetylation 98%, Mv = 1.61×10^5 g/mol), supplied by PARAFARM, Mar del Plata, Argentina was used as received. Glycerol (gly) purchased from SIGMA Aldrich was used as plasticizer. Ferric chloride ($FeCl_3 \cdot 6H_2O$), ferric sulfate ($FeSO_4 \cdot 7H_2O$) and sodium hydroxide were obtained from Aldrich.

2.2. Methods

2.2.1. Preparation of composite films

The films were prepared by casting, some of them containing glycerol in a wt. ratio glycerol/chitosan = 0.3. Chitosan solutions (2% wt/v) were prepared in aqueous acetic acid (1% v/v), by magnetic stirring during 1.5 h, adding the glycerol (if applicable) in the initial mixture. A 0.2 mol/L ferric salts solution was prepared by dispersing 9 g of ferric chloride with 4.62 g of ferric sulfate (Fe^{2+}:Fe^{3+} = 1:2 molar ratio) in 250 mL of aqueous acetic acid (1% v/v). An appropriate volume of the ferric salt solution (to obtain final films with 2–10 wt.% nanomagnetite) was then dispersed into the CS solution, by magnetic stirring during 10 min. The film-forming dispersions were defoamed under rest for one hour at room temperature and then poured into Teflon Petri dishes (diameter = 14 cm). Next, they were dried in a convective oven at 35 °C for 24 h, and finally kept under hood at room temperature for another day. The obtained films were peeled off from the plates and immersed in a NaOH aqueous solution (5 mol/L) during 0.5 h to induce the chemical co-precipitation of Fe^{2+} and Fe^{3+} ions, and then washed several times with distilled water until neutralization. Finally, the films were dried again under hood at room temperature and then kept in a closed container containing dried silica gel at room temperature (23 ± 2 °C) until testing.

2.2.2. Characterization of composite films

Magnetic characterization: The magnetic properties of magnetite/chitosan composites were obtained using a commercial SQUID magnetometer (Quantum Design, MPMS XL). In this way, both isothermal magnetization curves as well as Zero Field Cooling/Field Cooling (ZFC/FC) measurements were performed in order to characterize the magnetic properties of the nanocomposite films. The ZFC/FC measurement protocol was carried out as follows: the sample was first cooled down from 300 K to 5 K in zero magnetic field, then a static magnetic field of 50 Oe was applied and the magnetization was measured while increasing the temperature up to 300 K. Subsequently the sample was cooled down to 5 K under the same applied magnetic field (50 Oe) and the magnetization was measured while warming up the sample from 5 K to 300 K. Also, isothermal measurements were carried out at different temperatures between 2 and 300 K. Samples used for these tests were previously conditioned in a closed container with silica gel until they reached their equilibrium moisture content (about 5–7 wt.%).

Transmission electron microscopy (TEM): Transmission electron microscopy (TEM) was used to determine the morphology, size and distribution of the magnetite particles in the composite films. A JEOL 100 CX II (JAPAN, 1983) operating at 100 kV was used. The composite films were cut using an ultra-cryo-microtome and then placed onto the copper grids.

Small-angle X-ray scattering (SAXS): SAXS patterns of the nanocomposite films were performed on D1B-SAXS1 beamline at the Brazilian Synchrotron Light Laboratory (LNLS) in Campinas, Brazil. The measurements were carried out at room temperature. All data were collected using a 300 k Pilatus bidimensional detector and at a wavelength of λ = 1.822 Å. The scattering intensity was measured as function of momentum transfer vector q ($q = 4\pi \sin\theta/\lambda$), in a range from 0.06 to 6.0 nm^{-1}, being θ is the scattering angle.

3. Results and discussion

3.1. Magnetic behavior of non-plasticized films

Typically, the magnetic nanocomposite films of polymeric matrix have at least two different contributions that determine the magnetic properties of the material. One coming from the diamagnetic matrix and the other one from the super-paramagnetic nanoparticles included into it. Under the influence of an external magnetic field, diamagnetic materials generate small currents that oppose to the external field. This is the behavior found in the present work for the neat chitosan film and for the nanocomposite with low MNP content (2 wt.%) (curves not shown): they do not present a permanent magnetic moment under applied field [12] because the diamagnetic contribution of the matrix is the dominant magnetic effect, masking the magnetic behavior of the particles.

Changes in the magnetic behavior of the composite films containing relatively high percentages of magnetite nanoparticles are evident as can be seen in Fig. 1, which shows magnetization versus applied field for the non-plasticized samples containing 5 (CS-0gly-5MNP) and 10 (CS-0gly-10MNP) wt.% MNP (Fig. 1a and b, respectively) at 2 and 300 K. In order to display coercive field values, details of magnetization loops for low fields are shown in the inset of each figure. It is clear that both samples present absence of hysteresis at room temperature, whereas they have hysteresis (or are blocked) at 2 K. This behavior is the typical of a super-paramagnetic material. Table 1 summarizes the coercive fields for both samples at 2 and 300 K showing that these values increase as the temperature decreases. At the blocked regimen (low temperatures) the magnetic relaxation time is longer than the measurement time, the system is thermally blocked and the coercive field has a not null value. For higher temperatures, the magnetic relaxation time is shorter than the measurement time and an ensemble of single-core particles behaves as a super-paramagnetic material showing very low hysteresis effect and no residual magnetization [13,14].

Super-paramagnetic behavior is related to the sizes of the magnetic nanoparticles and the measurement time of the experimental technique used for its characterization, as indicated above. For example, if the particle size is reduced below a critical size (25 nm for magnetite particles [15]), and under certain experimental measurement time, much larger than the average relaxation time of the magnetic nanoparticles, the material becomes super-paramagnetic [13], i.e. the material behaves like a paramagnetic one (without hysteresis) but with a "super" or higher magnetic moment.

The magnetic properties obtained from the magnetization (M) vs field (H) curves of chitosan–magnetite films without plasticizer (glycerol) depend on Fe_3O_4 content as summarized in Table 1 and Fig. 1. For example, both samples (CS-0gly-5MNP and CS-0gly-10MNP) present a paramagnetic contribution at room temperature, with a more marked effect in the CS-0gly-5MNP sample. For the sample CS-0gly-10MNP a super-paramagnetic contribution evidenced by Langevin behavior is clear at room temperature [16]. On the other hand, for the CS-0gly-5MNP sample, the magnetization field behavior is far from a Langevin's one. Additionally, the shape of the magnetization loops at 2 K denotes a noticeable difference between both samples, where coercive field increases from 397.6 to 737.7 Oe as the content of MNP increases from 5 to 10 wt.% in the non-plasticized films. From Fig. 2, that shows the magnetization values at 20 KOe versus temperature, is also clear that the sample CS-0gly-10MNP presents higher values than those corresponding to the films containing lower concentration of magnetic particles in the whole range of temperatures analyzed.

For all the tested samples, the magnetization values at the highest field applied (20 KOe) close to room temperature (300 K) were much lower than those of bulk Fe_3O_4 (about 90 emu/g [17–19]) and spherical magnetite nanoparticles (i.e. 77.5 and 60.1 emu/g for nanomagnetite with average diameter = 11.5 nm at 5 and 300 K, respectively [20]). Considering that the iron oxide nanoparticles are embedded into a non-magnetic polymer matrix, the magnetization values of the composite films, which are related to the total mass, may include the magnetite (relatively low amount as compared with

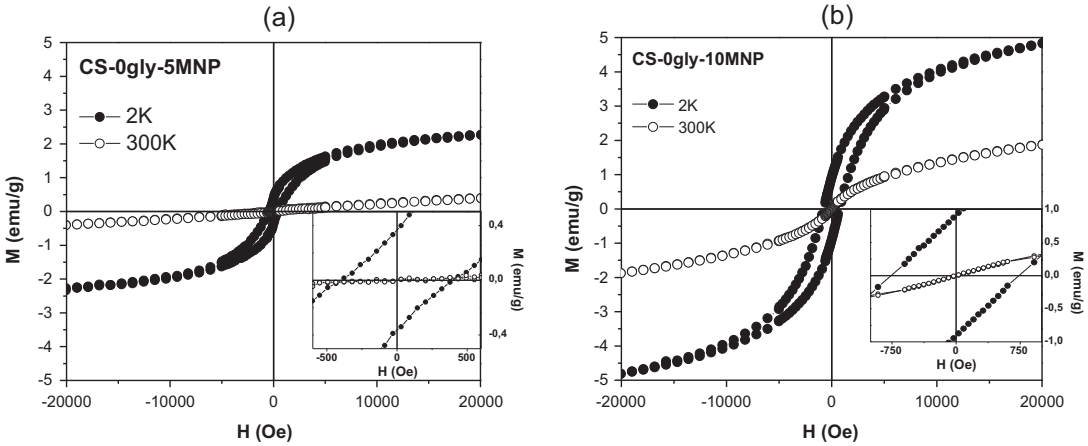

Fig. 1. Magnetization versus applied field curves at 2 K and 300 K for the non-plasticized samples containing 5 (a) and 10 wt.% MNP (b).

Table 1
Magnetization (M) and coercivity fields (Hc) for 2 and 300 K.

Nominal magnetite content	Glycerol content (wt.%)	*M* (H = 20,000 Oe) at 2 K (emu/g)	*M* (H = 20,000 Oe) at 300 K (emu/g)	Coercivity field Hc (*M* = 0) at 2 K (Oe)	Coercivity field Hc (*M* = 0) at 300 K (Oe)
2	0	–	–		
5		2.27	0.39	397.6	~0
7		2.86	0.64	418.2	~0
10		4.82	1.87	737.7	11.9
2	30				
5		0.28	0.022	1370.1	76.1
7		0.51	0.039	1587.1	77.6
10		0.81	0.086	1937.9	55.4

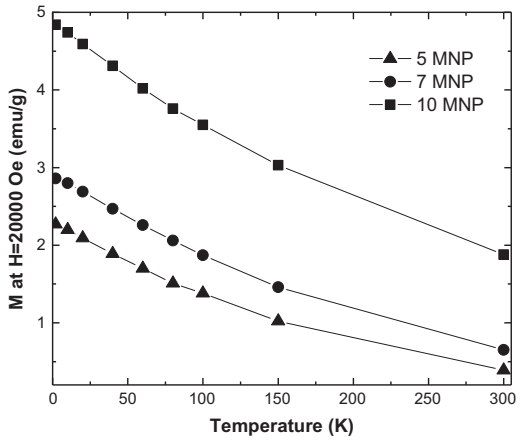

Fig. 2. Magnetization values at 20 KOe versus temperature for the non-plasticized films with 5, 7 and 10 wt.% MNP.

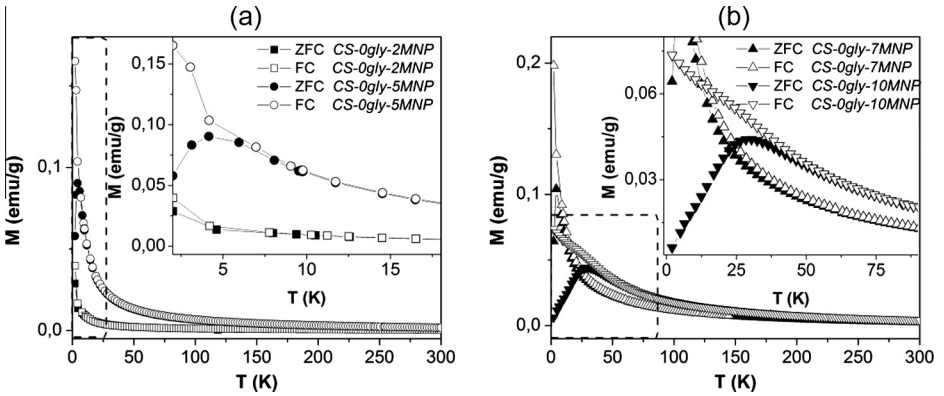

Fig. 3. Zero field cooling/field cooling measurements for the non-plasticized films. (a) 2 and 5 wt.% MNP; (b) 7 and 10 wt.% MNP.

the chitosan matrix) and the polymer (main constituent of the film) contributions. The correction of the magnetization values per mass of magnetite gives as a result of 45.4 emu/g and 48.2 emu/g at 2 K and 7.8 emu/g and 18.7 emu/g at 300 K for the CS-0gly-5MNP and CS-0gly-10MNP, respectively. The reduction of neat magnetization could be attributed to different effects like surface disorder and low crystallinity of the magnetic particles, as indicated by Moscoso-Londoño et al. [21], but also possibly to particle agglomeration into the film that increase the effective particle size, perhaps above the critical one, reducing even more the amount of super-paramagnetic particles in the film. In this way, it is understandable that the saturation magnetization values of the composites are lower than that of the well-crystallized bulk magnetite nanoparticles, as was noticed by other researchers [1,22,23]. Moreover, it is clear that the polymeric diamagnetic matrix also influences the particle magnetic behavior, perhaps restricting their ability to grow or crystallize, since the corrected magnetization values, especially those calculated at 300 K, depend strongly on the particle content in the films.

The zero field cooling/field cooling measurements were carried out to better understand the magnetic properties of these materials (Fig. 3). From these measurements is possible to obtain the temperature at which the system undergoes from blocked to super-paramagnetic regimen. This temperature is called blocking temperature, T_B, and can be considered as the threshold where the thermal energy overcomes the energy barrier related to the change in the orientation of the magnetic moment [24]. The 2 wt.% MNP film does not evidence a blocking temperature, possibly due to the high contribution of the diamagnetic matrix (due to the low concentration of magnetic particles), which masks the super-paramagnetic behavior of the particles (Fig. 3a).

The samples with 5, 7 and 10 wt.% of MNP exhibited the same trend in FC and ZFC curves (Fig. 3b), and a maximum in the ZFC curve (blocking temperature, T_B) was observed. The samples containing 5 and 7 wt.% MNP have blocking temperatures around 4 K and with small differences respect to the values of the irreversibility ones, T_i (defined as the threshold temperature above which FC and ZFC curves coincide), indicating non-dipolar interaction between the nanoparticles. From these small differences between T_B and T_i we can infer also that the nanoparticles dispersed in these films have a narrow size distribution. Moreover, at temperatures higher than the blocking one a typical Curie Weiss behavior can be noticed, confirming the non-interaction between the MNP [16]. On the other hand, the T_B of the sample with 10% MNP is higher, showing a value of 26 K and higher differences with its T_i (35 K, Fig. 3b). Blocking temperature value is associated with the particle size distribution through anisotropy density (kV, being K the magnetic anisotropy constant). Thus, as higher is the average volume of the particles (V) higher is T_B. Hence, the higher T_B of the sample containing 10 wt.% MNP (CS-0gly-10MNP) respect to the less concentrated ones suggests that nanoparticle volume in the former sample is higher than those of films containing 5% or 7%. Due to the increase of particle sizes, also dipolar interaction (due to agglomeration of the nanoparticles on the film) became more relevant and could be the reason of the large difference between the T_B and T_i noticed in the CS-0gly-10MNP sample.

3.2. Magnetic behavior of plasticized films

The fragility of the films increases as the iron salts concentration increases, leading to totally brittle materials that break easily and cannot be manipulated without cracking for concentrations of 7 wt.% MNP and higher. For this reason, a new series of nanocomposite films was prepared by using glycerol as a plasticizer, which was selected due to its plasticizing power, non-toxicity and thermal stability [25]. Thus, in this case, quite flexible films were obtained even using 10 wt.% magnetite [11].

Fig. 4 and Table 1 shows magnetization field dependence measurements for the films with different content of MNP and 30 wt.% of glycerol. In comparison with the non-plasticized films, the hysteresis loops of the curves obtained at room temperature are broader, which could be explained either by accepting a worst dispersion and more interaction (agglomeration) among magnetic particles or that the average particle size of the precipitated nanomagnetite into the plasticized films is larger than that achieved in the films containing no glycerol. This difference with the behavior of non-plasticized films is more pronounced at low temperatures, when the nanoparticles are in the blocked state. Also, it is interesting to notice that for the sample with 5 wt.% MNP (CS-30gly-5MNP) the magnetization loops evidence two magnetic contributions. This is clear from the slop change near ±5 KOe for the measurement at 2 K and near 500 Oe from the measurement at 300 K (see inset). These contributions could be due to two different nanoparticles sizes and/or others possible effects like aggregation, surface effects (that results from the symmetry breaking of the crystal structure at the surface of the particle), oxidation, dangling bonds, surface strain, or different chemical and physical structures of internal "core" and surface "shell" parts of the nanoparticle [26]. These effects could magnetically harden the materials leading to an increase in the coercive field.

Moreover, the results denote that the presence of glycerol in the films decreases significantly the magnetization value at 20 KOe in comparison with the non-plasticized films (Table 1). In addition, the saturation magnetization is not reached for any of these samples in the range of fields evaluated and, for all temperatures, a marked paramagnetic contribution is observed (Fig. 4). The paramagnetic contribution, which turns up clearer in the more concentrated samples (10 wt.%), could be associated to the presence of Fe (II) and Fe (III) (from the ferric salts solutions used at the initial step of the composite preparation) that did not precipitate into magnetite. In the present case (composite films prepared by the "in situ" formation of magnetic particles) the presence of iron residual salts (i.e. salts formed during the chemical co-precipitation that could have been retained inside the composite film after the washing steps) and the contribution of surface effects that affect the spin order, originated mainly in the presence of a distribution of particle sizes and due to the interaction of the particles with the support matrix [16] could also affect the magnetic behavior. Moreover, the presence of glycerol would delay the precipitation of magnetite into the films generating iron rich regions that, when precipitate, lead to larger particle sizes than those obtained in non-plasticized films. Contrary, in absence of glycerol the salts would be more uniformly distributed allowing the formation of more nucleation cores that would grow into more uniform but smaller nanoparticles.

ZFC/FC measurements confirm the existence of two magnetic contributions (Fig. 5) on the plasticized nanocomposite films with 30 wt.% of glycerol. For the sample containing 2 wt.% MNP a T_B of about 4 K is observed. On the other hand, for the samples with 5, 7 and 10 wt.% MNP the two blocking temperatures (T_{B1} and T_{B2}) observed are associated to the presence of two well distinguished sizes of the particles embedded in these films, effect not common. The first maximum in the ZFC curves, T_{B1}, appears at 6.4 K for the three samples, while the second one, T_{B2}, depends on the content of MNP and thus appears at 18, 24 and 32 K for the samples with 5, 7 and 10 wt.% of MNP, respectively. The shifting of the maximum in the ZFC curves to higher temperatures could be attributed to a slight increase in the sizes of the precipitated magnetic

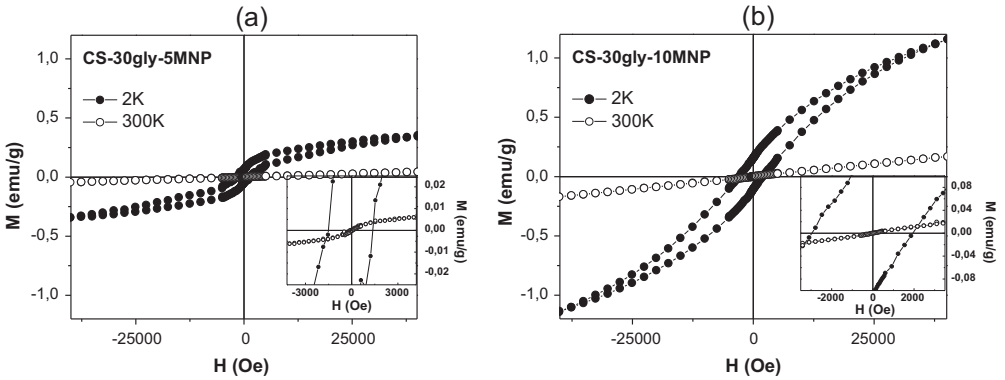

Fig. 4. Magnetization versus applied field curves at 2 K and 300 K for the plasticized samples containing 5 (a) and 10 wt.% MNP (b).

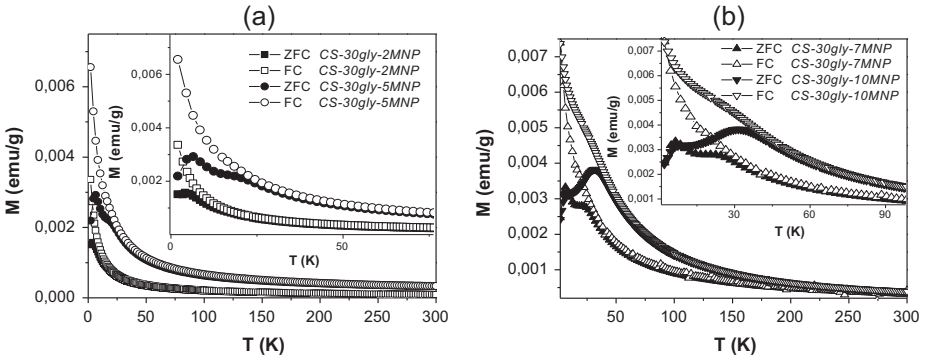

Fig. 5. Zero field cooling/field cooling measurements for the plasticized films. (a) 2 and 5 wt.% MNP; (b) 7 and 10 wt.% MNP.

nanoparticles. Moreover, for plasticized chitosan films, T_i presents a linear relationship with the content of MNP, as can be observed in Fig. 6, evidencing a well defined tendency.

Thus, it is clear that the use of glycerol in the film forming solutions promotes bimodal distribution of MNP in the plasticized chitosan matrix, which could be related to its phase separated film structure. As was stated in previous works [25], glycerol plasticized chitosan films develop a two separated phase structure formed by soft glycerol-rich and rigid chitosan-rich domains, which present characteristic relaxation processes occurring at low (about −30 °C) and high temperatures (about 35 °C), respectively. In this sense it could be conjectured that the size of the precipitated nanomagnetite strongly depend on the phase where it grows. Thus, considering both the results of the previous section (no glycerol-rich phase) with

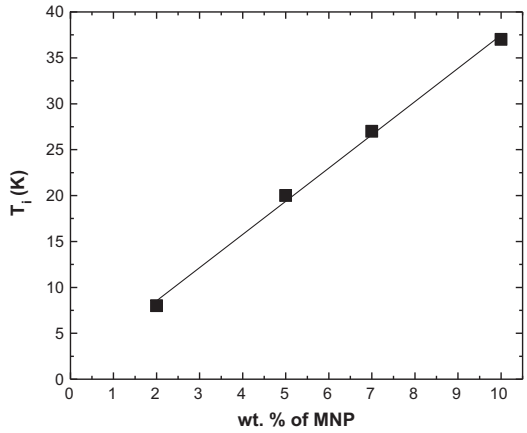

Fig. 6. Temperature of irreversibility (T_i) as a function of the MNP content.

the fact that this new phase is softer than chitosan rich one, it can be concluded that larger magnetite particles would grow in the glycerol rich domains. Moreover, inside this soft phase the diffusion/movement of particles should be easier than in the chitosan rich domains and thus, particle agglomeration also could occur.

The presence of bimodal nanoparticles distribution is almost not reported in the bibliography and is very promising from technological point of view. Considering that the nanoparticles can be thermally activated with a radio-frequency external magnetic field, and this activation depends on nanoparticles sizes, these systems could offer two possible work regimes associated to the two nanoparticles sizes.

3.3. TEM and SAXS results

To complement the previous results and corroborate the hypothesis raised about particle sizes, TEM micrographs of selected samples were obtained. Fig. 7 shows the images CS-30gly-2MNP, CS-0gly-5MNP, CS-30gly-5MNP and CS-30gly-7MNP films obtained at 200,000× magnification. It can be noticed that nanoparticles are separated each other in diluted systems (Fig. 7a, from CS-30gly-2MNP), with diameters ranging from 5 to 13 nm, as reported in a previous publication [11]. As the magnetite concentration in the films increases, more complex structures (Fig. 7b–d), probably fractal organizations, are observed. The number of these structures increases for the plasticized films, as can be concluded from the comparison of Fig. 7b and c, both samples containing 5% MNP. This could be due to the accumulation of magnetic particles/nuclei in certain regions (more probably glycerol-rich ones), which in turn would lead to an increase in the particle size.

Also, small-angle X-ray scattering (SAXS) studies were performed to determine both the radius of gyration and the fractal dimension of the nanocomposites. Plasticized films containing 5 and 7 wt.% MNP were selected to perform a semi-quantitative analysis. Fig. 8a shows the Log–Log plot of $I(q)$ vs. q for the nanocomposites under study. As it is clearly noted, SAXS experimental curves display three different scattering regions, according to the q region considered. In low-q region, both spectra display power law behavior and thus, they were fitted using the form:

$$I(q) = I_0 * q^{-\alpha} \tag{1}$$

where I_0 is a constant and α is related to the correlation length on the material [21,27]. The values of the exponent obtained were −1.1 and −1.3 for samples with 5 and 7 MNP, respectively.

At high q, the scattered intensity decays with a slope of −2 for both samples, which is related to the mass fractal structure of the aggregates through the equation:

$$I(q) = B_2 * q^{-Df} \tag{2}$$

where D_f is the mass-fractal dimension and B_2 is the law pre-factor. The fact that the two samples with different concentrations of nanoparticles have the same slope suggests that the primary particle organization in the fractal structures does not depend on the nanoparticle content [28]. Finally, the shoulder in the central region would correspond to inter-particle scattering from magnetite nanoparticles [29].

To obtain more information about these systems, Guinier plots (Eq. (3)) were also constructed and they are shown in Fig. 8b.

$$\ln I \ vs \ q^2 \tag{3}$$

The concave form of the curves is an indicative of polydispersity, meaning that there is a characteristic length of the constituent in each sample elements. At lower values of q (in the linear region), the radius of gyration (Rg) of the scattering objects could be estimated by using the following formula [24]:

$$I(q) = G\exp(-q^2Rg^2/3) \tag{4}$$

In this way, the radii of gyration obtained were 11.49 nm and 10.55 nm for the samples with 5 and 7 MNP, respectively. Then, assuming that the nanoparticles are spherical, their average diameters can be calculated using

$$D = 2(5/3)^{1/2}Rg \tag{5}$$

The calculation led to particle diameters of 29.66 and 27.24 nm, for CS-30gly-5MNP and CS-30gly-7MNP films, respectively (Table 2). Then, taking into account the results of TEM images, it is clear that these values correspond to particle agglomerates instead of individual nanoparticles. However, it should be considered that in this work q was varied from 0.05 to 1.3 nm^{-1} and thus, nanoparticles with sizes below 6 nm approximately cannot be detected.

Although the size of the agglomerates/fractal structures do not match exactly the measurements in the TEM images, is should be taken into account that TEM analysis involves a very limited region of the composite film while SAXS gives us averaged results of an area sample of around mm^2. In this sense we can conclude that both techniques allow us to corroborate the existence of fractal structures/agglomerates of larger sizes as compared with individual nanomagnetite particles.

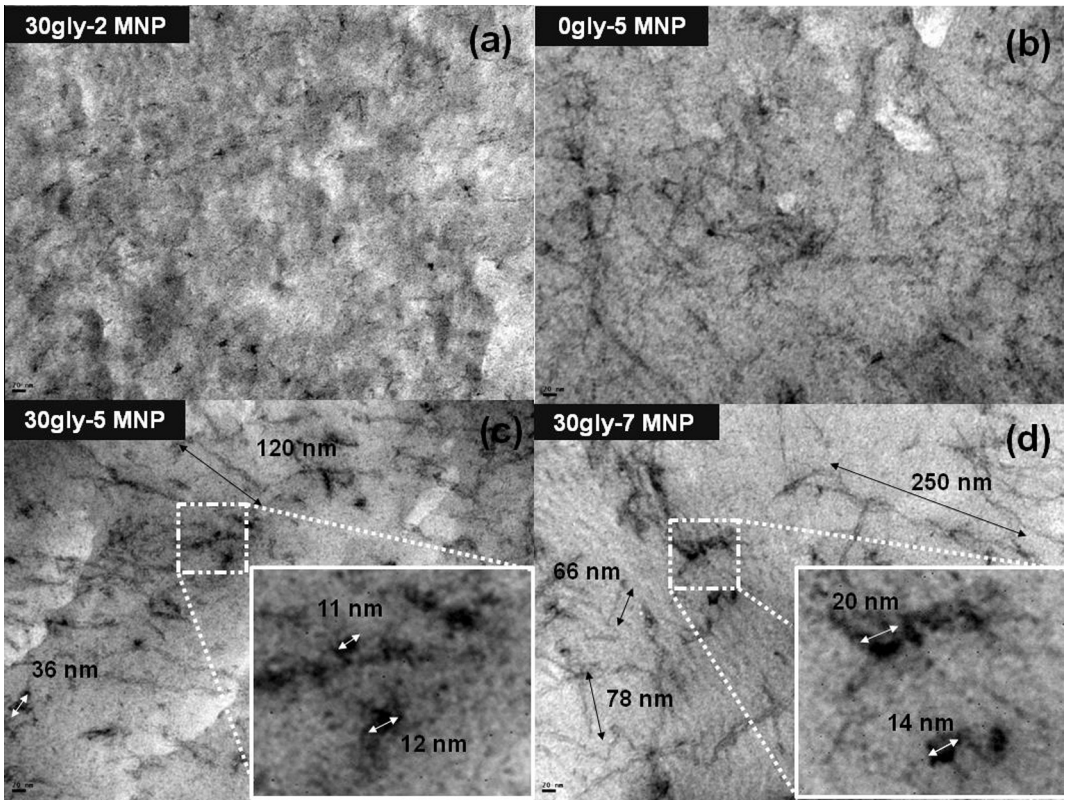

Fig. 7. TEM micrographs of the nanocomposite films. (a) 30gly-2MNP; (b) 0gly-5MNP, (c) 30gly-5MNP, (d) 30gly-7MNP.

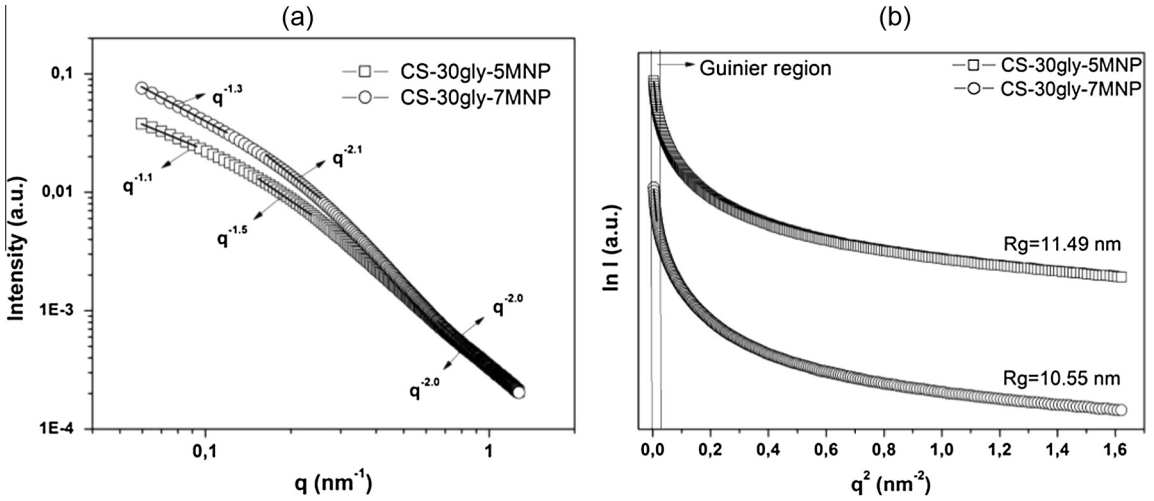

Fig. 8. (a) Small angle X-ray scattering intensity (I) as function of the momentum transfer vector (q) for plasticized samples containing 5 and 7 wt.% MNP, (b) Guinier curves (ln I vs q^2) of plasticized samples containing 5 and 7 wt.% MNP.

Table 2
Radii of gyration (Rg) and average diameters (D) of the plasticized films with 5 and 7 wt.% MNP.

	CS-30gly-5MNP	CS-30gly-7MNP
Rg (nm)	11.49	10.55
D (nm)	29.66	27.24

4. Conclusions

Complex chitosan-plasticized and non-plasticized films loaded with magnetite nanoparticles precipitated "in situ" were successfully obtained by solvent-casting. Nanocomposite films with nanomagnetite concentrations higher than 2 wt.% exhibit super-paramagnetic behavior, which in turn depends strongly on the magnetic particles content and size and on the presence of plasticizer. In general low concentrated samples present a low blocking temperature, which was related with a small particle or small agglomerated size, while the higher concentrated ones present a higher T_B (non-plasticized films) or two different T_B appearing at low and high temperatures (plasticized samples), indicating a bimodal particle size distribution. This last effect was explained considering the two-phase structure of plasticized chitosan films and it is an interesting characteristic that could be used in technological applications where two work regimes, associated to the two magnetic nanoparticles sizes, were required. The size of the particles or the agglomerates precipitated into the films was corroborated by TEM and SAXS measurements and a fractal association was proposed for the particles precipitated into plasticized films.

Acknowledgements

The authors gratefully acknowledge the financial support provided by the National Research Council (CONICET, Grant PIP 0637), the Science and Technology National Promotion Agency (ANPCyT, Grant PICT-2013-1535) and the National University of Mar del Plata (Project # 15/G430) from Argentina. The work at UNICAMP was supported by FAPESP (2011/1234-6) and CNPq (Project # 506394/2013-1) from Brazil. Small-angle X-ray scattering data were acquired at beamline D1B-SAXS1 (17036) at Brazilian Synchrotron Light Laboratory (LNLS).

References

[1] A.S. Bhatt, D. Krishna Bhat, M.S. Santosh, Electrical and magnetic properties of chitosan–magnetite nanocomposites, Physica B 405 (2010) 2078–2082.
[2] Y. Zhang, C. Xue, Y. Xue, R. Gao, X. Zhang, Determination of the degree of deacetylation of chitin and chitosan by X-ray powder diffraction, Carbohydr. Res. 340 (2005) 1914–1917.
[3] C. Yuwei, W. Jianlong, Preparation and characterization of magnetic chitosan nanoparticles and its application for Cu(II) removal, Chem. Eng. J. 168 (2011) 286–292.
[4] Z. Karimi, L. Karimi, H. Shokrollahi, Nano-magnetic particles used in biomedicine: core and coating materials, Mater. Sci. Eng. C 33 (2013) 2465–2475.
[5] B.L. Cushing, V.L. Kolesnichenko, C.J. O'Connor, Recent advances in the liquid-phase syntheses of inorganic nanoparticles, Chem. Rev. 104 (2004) 3893–3946.
[6] S.Y. Shim, D.K. Lim, J.M. Nam, Ultrasensitive optical biodiagnostic methods using metallic nanoparticles, Nanomedicine 2 (2008) 215–232.
[7] A.P. Safronov, I.V. Beketov, I.S. Tyukova, A.I. Medvedev, O.M. Samatov, A.M. Murzakaev, Magnetic nanoparticles for biophysical applications synthesized by high-power physical dispersion, J. Magn. Magn. Mater. 383 (2015) 281–287.
[8] J.K. Oh, J.M. Park, Iron oxide-based superparamagnetic polymeric nanomaterials: design, preparation, and biomedical application, Prog. Polym. Sci. 36 (2011) 168–189.
[9] V. Salgueirino-Maceira, M.A. Correa-Duarte, Increasing the complexity of magnetic core/shell structured nanocomposites for biological applications, Adv. Mater. 19 (2007) 4131–4144.
[10] A.K. Gupta, R.R. Naregalkar, V.D. Vaidya, M. Gupta, Recent advances on surface engineering of magnetic iron oxide nanoparticles and their biomedical applications, Nanomedicine 2 (2007) 23–39.
[11] G.A. Kloster, N.E. Marcovich, M.A. Mosiewicki, Composite films based on chitosan and nanomagnetite, Eur. Polym. J. 66 (2015) 386–396.
[12] K.Y. Castrejón-Parga, H. Camacho-Montes, C.A. Rodríguez-González, C. Velasco-Santos, A.L. Martínez-Hernández, D. Bueno-Jaquez, J.L. Rivera-Armenta, C.R. Ambrosio, C. Chapa Conzalez, M.E. Mendoza-Duarte, P.E. García-Casillas, Chitosan–starch film reinforced with magnetite-decorated carbon nanotubes, J. Alloys Compd. 615 (2014) S505–S510.
[13] L. Neel, Theorie du trainage, magnetique des ferromagnetiques en grains fins avec applications aux terre cuites, Annls Geophys. 5 (1949) 99–136.
[14] L. Néel, Propriétés magnétiques des ferrites: ferrimagnétisme et antiferromagnétisme (Magnetic properties of ferrites: ferrimagnetism and antiferromagnetism, Ann. Phys. 3 (1948) 137–198.
[15] Q. Hu, F. Chen, B. Li, J. Shen, Preparation of three-dimensional nano-magnetite/chitosan rod, Mater. Lett. 60 (2006) 368–370.
[16] R.H. Kodama, Magnetic nanoparticles, J. Magn. Magn. Mater. 200 (1999) 359–372.
[17] S. Chikazumi, Physics of Magnetism, Wiley, New York, 1964. p. 100.
[18] M. Mikhaylova, D.K. Kim, N. Bobrysheva, M. Osmolowsky, V. Semenov, T. Tsakalakos, M. Muhammed, Superparamagnetism of magnetite nanoparticles: dependence on surface modification, Langmuir 240 (2004) 2472–2477.
[19] R. Cornell, U. Schwertmann, The Iron Oxides: Structure, Properties, Reactions, Occurrences and Uses, Wiley-VCH Verlag GmbH & Co. KGaA, Weinheim, 2003.
[20] G.F. Goya, T.S. Berquó, F.C. Fonseca, M.P. Morales, Static and dynamic magnetic properties of spherical magnetite nanoparticles, J. Appl. Phys. 94 (5) (2003) 3520–3528.
[21] O. Moscoso-Londoño, J.S. Gonzalez, D. Muraca, C.E. Hoppe, V.A. Alvarez, A. López-Quintela, L.M. Socolovsky, K.R. Pirota, Structural and magnetic behavior of ferrogels obtained by freezing thawing of polyvinyl alcohol/poly(acrylic acid) (PAA)-coated iron oxide nanoparticles, Eur. Polym. J. 49 (2013) 279–289.
[22] J. Yang, S.B. Park, H.G. Yoon, Y.M. Huh, S. Haam, Preparation of poly ε-caprolactone nanoparticles containing magnetite for magnetic drug carrier, Int. J. Pharm. 324 (2006) 185–190.
[23] L. Cui, H. Gu, H. Xu, D. Shi, Synthesis and characterization of superparamagnetic composite nanorings, Mater. Lett. 60 (2006) 2929–2932.
[24] A. Labarta, X. Batlle, O. Iglesias, From finite size and surface effects to glassy behaviour in ferrimagnetic nanoparticles, chapter 4 in the book: "Surface effects in magnetic nanoparticles", in: D. Fiorani (Ed.), Nanostructured Science and Technology Series, Springer Science+Business Inc., Nueva York, 2005.
[25] M. Pereda, A. Dufresne, M.I. Aranguren, N.E. Marcovich, Polyelectrolyte films based on chitosan/olive oil and reinforced with cellulose nanocrystals, Carbohydr. Polym. 1011 (2014) 1018–1026.
[26] B. Issa, I.M. Obaidat, B.A. Albiss, Y. Haik, Magnetic nanoparticles: surface effects and properties related to biomedicine applications, Int. J. Mol. Sci. 14 (11) (2013) 21266–21305.
[27] G. Beaucage, H.K. Kammler, S.E. Pratsinis, Particle size distributions from small-angle scattering using global scattering functions, J. Appl. Crystallogr. 37 (2004) 523–535.

[28] R. Hernández, J. Sacristán, L. Asín, T.E. Torres, M.R. Ibarra, G.F. Goya, et al, Magnetic hydrogels derived from polysaccharides with improved specific power absorption: potential devices for remotely triggered drug delivery, J. Phys. Chem. B 114 (2010) 12002–12007.
[29] A. Millan, F. Palacio, A. Falqui, E. Snoeck, V. Serin, A. Bhattacharjee, et al, Maghemite polymer nanocomposites with modulated magnetic properties, Acta Mater. 55 (2007) 2201–2209.